Turbulence, Heat and Mass Transfer 7
© 2012 Begell House, Inc.

Flow Observation and Heat Transfer Performance of Viscoelastic Fluid Flow in a Serpentine Channel

K. Tatsumi[1,2], O. Nakajima[1], W. Nagasaka[1] and K. Nakabe[1,2]
[1]*Department of Mechanical Engineering and Science, Kyoto University, Yoshida-honmachi, Sakyo-ku, Kyoto 606-8501, Japan, tatsumi@me.kyoto-u.ac.jp*
[2]*Advanced Research Institute of Fluid Science and Engineering, Kyoto University, Yoshida-honmachi, Sakyo-ku, Kyoto 606-8501, Japan*

Abstract –This paper describes the results of heat transfer, flow visualization and PIV measurements conducted for the viscoelastic fluid flow in a serpentine channel with square cross-section under low Reynolds number conditions. Polyacrylamide water solution was used as viscoelastic fluid, and was compared with the results of Newtonian fluid. In the visualization, flow fluctuations and secondary flows did not appear in the Newtonian fluid case. On the other hand, unsteady flow and longitudinal vortices were observed in the viscoelastic fluid case. The velocity fields showed that large flow fluctuations were generated in the downstream area of the inflection point of the serpentine channel. Single or a pair of longitudinal vortices was generated in this area. The generation of these vortices can be attributed to the normal stress produced by the viscoelasticity of the fluid and the curvature of the channel. Considerable enhancement of heat transfer performance was obtained by the flow fluctuation and longitudinal vortices.

1. Introduction

Applying the viscoelastic fluid as a working fluid in the channel flow is considered to be an alternative solution to the geometrical and mechanical modification of the channel for heat transfer enhancement [1,2]. The high shear stress generated in the channel will cause the polymers solved in the fluid to contract and expand leading to an appearance of the elasticity and additional normal stresses in the flow. In combination with a certain flow pattern, this elasticity of the fluid increases the flow instability resulting in generation of an unsteady flow (viscoelastic turbulence) even in low Reynolds number regime [3,4].

Recently, several studies on the mixing characteristics of viscoelastic fluid in a serpentine-curved channel under low Reynolds number condition have been published in the literatures. Groisman & Steinberg (2001) carried out flow visualization and point measurement of the flow velocities using laser Doppler anemometer. Flow fluctuation was observed even in the order of $Re \sim 10$, accompanying the enhancement of the fluid mixing. Teodor et al. (2004) conducted a visualization experiment in serpentine microchannels using fluorescent dye. Even in this scale, production of the unsteady flow and enhancement in the fluid mixing was observed. Tamano et al. (2009) made PIV measurements in curved channels with circular cross-section and found a pair of vortices similar to the Taylor vortices in the time-mean velocity fields. These results show that considerable fluctuations can be obtained in such flows suggesting the possibility of enhancing the mixing performance or, moreover, mass and heat transfer at the channel wall effectively. To the knowledge of the authors, however, there are no experiments conducted to link the viscoelastic turbulence with heat transfer performance in serpentine channels. It is essential to understand the turbulence and heat transfer characteristic of such flows in order to provide insights for evaluating the

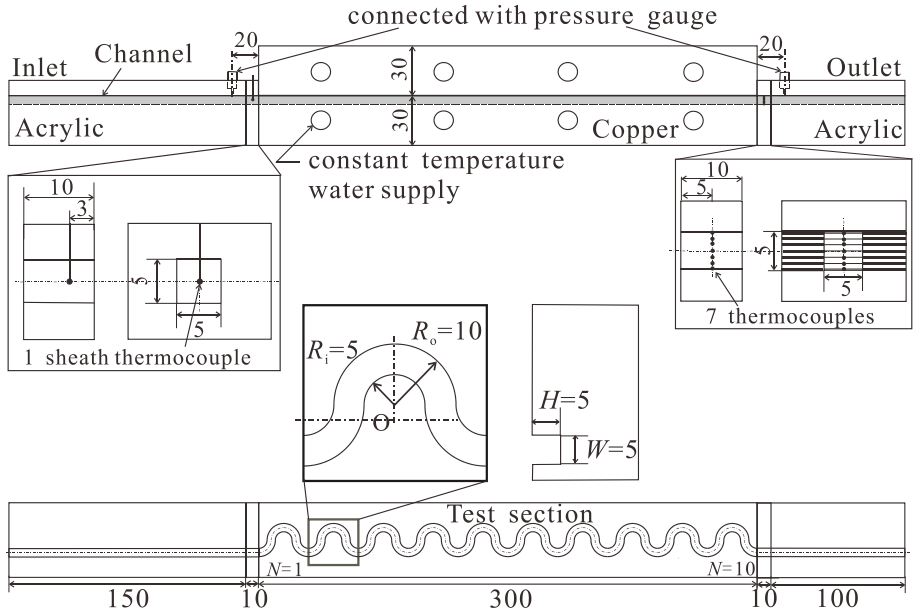

(a) Heat transfer measurement

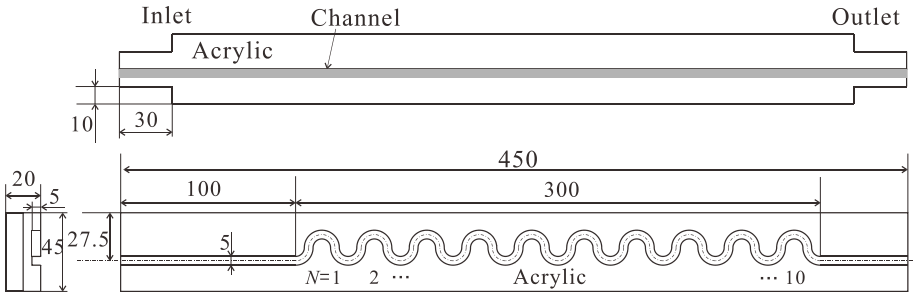

(b) Flow visualization and PIV measurements

Figure 1: Experimental apparatus used for the heat transfer measurement, flow visualization and PIV measurement.

feasibility and designing of effective channel shape for practical use in thermal engineering.

From this background, measurement of the heat transfer coefficient under isothermal wall condition was carried out in the serpentine channel, the schematic of which is shown in Fig. 1. Flow visualization and velocity measurement were carried out by supplying dye to the flow and using the particle image velocimetry (PIV) in order to understand the flow behavior. Two types of working fluids were investigated. One was a viscoelastic fluid of 64wt% sucrose water solution to which polyacrylamide of 500ppm was added, and the other was a Newtonian fluid of a sucrose water solution.

2. Experimental Procedures

Figure 1 shows the schematic diagram of the experimental apparatus applied to the measurements. The channel consisted of three parts: the inlet and outlet channel parts, and the test section, the channel shape of which is a serpentine one with semicircle curves. In the heat transfer measurement, the walls of the test section were heated under isothermal condition. The working fluid was supplied to the channel by a pump driven by pressurized air. The mass flow rate was measured by measuring the mass of the fluid flowing out from the outlet of the channel using an electronic balance, the accuracy of which was 0.01g. The mass of the fluid changed linearly during the measurement, and the time average value was used to obtain the

average volume flow rate, the accuracy of which was 0.3ml/min.

For the heat transfer measurement, the inlet and outlet units were made of acrylic, to which a straight channel was embedded. The test section was made of copper in order to produce an isothermal condition to the wall. As shown in Fig. 1 (a), cylindrical channels were transversely drilled to the wall to which constant temperature water was supplied from the thermostat bath to keep the wall temperature of the channel constant. The inlet and outlet parts were attached to the test section and sealed with silicon sealant. For the flow visualization and PIV measurement, the channel made of transparent acrylic was used. 5mm holes were drilled through the walls located at the end of the channels. Tubes were connected to these holes supplying fluids to the channel from the pump, and leading the outlet fluid to a container to measure the mass flow rate.

The schematic and dimensions of the serpentine channel are shown in the lower part of Figures 1 (a) and (b). The channel had a square cross-section of 5mm in width and height. The serpentine channel had a periodical shape, which consisted of 10 repeating units of circular curved parts. The inner and outer radii were 5 and 10mm, respectively.

2.1 Heat transfer measurements

In order to measure the fluid temperature for bulk mean temperature calculations, temperature measurement units were placed at the inlet and outlet of the cupper test section. The fluid temperature at the inlet, $T_{b,i}$, was measured by a sheath K-type thermocouple of 0.5mm in diameter having its end point positioned at the center of the channel cross section. Temperature at a single point only was measured since a uniform temperature distribution was expected for the inlet flow. The fluid temperature at the outlet $T_{b,o}$ was measured by 7 K-type thermocouples located evenly in the height direction in the middle of the channel width. Since the available temperature distributions obtained from this measurement were only in one-dimensional form, expansion of the temperature distribution from one- to two-dimensional directions was necessary. Thus, in this study, the fluid temperature was assumed to have a similar distribution in the y and z directions to the one measured at $z = 0$. The temperature of the heated cupper part was measured by K-type thermocouples, which were embedded in the cupper surface. The variation of the temperature was 0.5 °C affirming that a constant wall temperature condition was obtained at the channel.

In combination with the measured temperature mentioned in above, the streamwise velocity distributions of a square cross-section in a laminar flow case (Shah, 1978) were used in the sucrose solution case in order to obtain the bulk mean temperatures of fluids at the inlet and outlet. In the PAAm solution case, the velocity distribution was calculated on the basis of the following procedure. First, we will use the velocity distribution of the power law fluid for the flow in a circular duct shown by Wiginton and Dalton (1970).

$$\frac{u}{U_m} = \frac{3n+1}{n+1}\left[1-\left(\frac{r}{a}\right)^{\frac{n+1}{n}}\right] \tag{1}$$

In order to convert this equation to the velocity distribution of a flow in a square duct, the difference between the velocity distributions of flows in circular and square ducts of Newtonian fluid is calculated and, then, multiplied to the Eq. (1). The result is shown in Eq.(2).

Table 1: Flow conditions of the heat transfer experiment.

Fluid	U_m [mm/s]	*Re*	N_D	*Wi*
Sucrose	10 – 40	0.82 – 2.4	0.1 – 0.5	–
PAAm	10 – 81	0.30 – 2.64	0.05 – 0.49	14.2 – 140

$$\frac{u}{U_m} = \left[0.1438r_a^4 - 0.334r_a^3 + 0.2829r_a^2 + 0.0161r_a + 1.0577\right] \times \frac{3n+1}{n+1}\left[1-\left(\frac{y}{2.5}\right)^{\frac{1.2n+1}{n}}\right]\left[1-\left(\frac{y}{2.5}\right)^{\frac{1.2n+1}{n}}\right] \tag{2}$$

where $r_a = y/25 = z/2.5$. The velocities obtained from Eq. (2) and the temperature distribution were employed to calculate the bulk mean temperatures in the viscoelasic fluid flow case.

The average heat transfer coefficient was then calculated on the basis of the logarithmic temperature difference as shown by Eq. (3).

$$\bar{h} = \frac{\dot{m}c_p}{A_s} \times \ln \frac{T_w - T_{b,i}}{T_w - T_{b,o}} \tag{3}$$

where $\dot{m}$ and A_s are the mass flow rate and the heat transfer area.

2.2 Pressure loss measurement

To measure the pressure loss in the test section, electronic pressure gauges (Keyence Co., AP-C30), the measurement resolution of which was 0.1kPa, were connected to the inlet and outlet of the test section through a 1mm hole drilled at the top wall as shown in Fig. 1 (a). The static pressure at each position was measured and used to calculate the fanning friction factor, f , defined as Eq. (4) .

$$f = \frac{2\Delta P}{\rho U_m^{\ 2}} \frac{D_h}{4L} \tag{4}$$

D_h and L are the hydraulic diameter and channel length, respectively. U_m is the mean velocity.

2.3 Flow visualization

Flow visualization using dye was carried out in this study to understand the flow behavior in the channel. Syringe pump (Harvard apparatus., econoflo) was used to supply the ink though a 4mm inner diameter tube to a syringe needle, which was inserted to the channel through the top wall. The images of the visualization were recorded using two digital video cameras (Sony, HDR-CX370V) measured from above and side of the channel simultaneously.

2.4 PIV measurement

The PIV system was composed of a double pulse Nd:YAG laser (New Wave Solo3: wave length 532nm), high resolution CCD camera (TSI, Powerview Plus 4MP: 12-bit monochrome, 4-Mpixels) and a synchronizer (TSI, 610034). The spatial resolution of the image obtained by the camera in combination with the lens (Nikon Co., AF-Zoom-Nikkor 24-85mm) was 15μm/pixels. The frame rate of the measurement was 5 frames/s. 50 pairs, which was 10s converted in time, of the images were recorded 12 times during the measurement. Therefore,

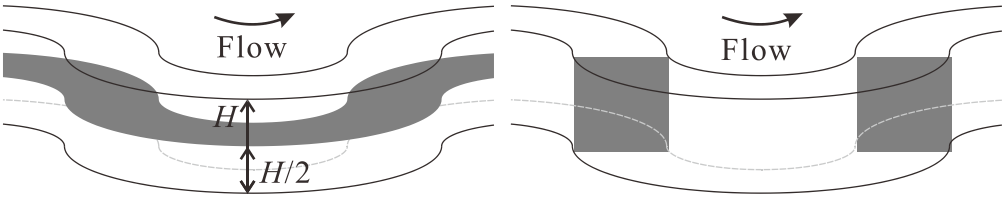

(a) Measured from above (x-y plane) *(b) Measured from side (r-z plane)*

Figure 2: The planes of the velocity fields measured by the PIV (laser sheet positions).

the total time was 120s, a period of which was sufficiently long to calculate the time average values of the velocity and fluctuation quantities. PIV analysis software (TSI, Insight 6.0) was used to calculate and analyze the velocity distribution from the recorded images. For the PIV measurement, glass beads (La Vision, glass hollow sphere) with nominal diameter of 10μm were mixed in the fluids as tracer particles. The concentration of the particles was 0.016wt%.

The velocity fields were measured from two directions as depicted by the schematic diagram shown in Fig. 2. One was from the top of the channel and the other was from the side of the channel. For the *x–y* plane, measurement was made at the middle of the channel height ($z = 0.5H$). For the *x–z* plane, measurement was carried out so that the plane crossed the inflection point of the curved channel. Therefore, as shown in the Fig. 2(b), velocity fields at two cross-sections, which were the upstream and downstream sides of the semi-circle, were obtained. The thickness of the laser sheet was approximately 0.5mm.

2.5 Working fluid preparation

Two kinds of working fluids were prepared for the measurement. One was a sucrose water solution (sucrose 64.4wt%), which was a Newtonian fluid. The other was the polyacrylamide (PAAm) water solution (sucrose 64,4wt%, NaCl 1wt%, PAAm 500ppm), which was a viscoelastic fluid. NaCl was mixed in the fluid to keep the polymer structure and fluid properties stable. The fluids were prepared mixing the solute to water using a pot rotating mill. Measurement was carried out within three days the working fluid was prepared confirming that degradation of the fluid was not observed within this period.

The fluid density ρ, viscosity μ and relaxation time λ were measured prior to the experiment. μ and λ were measured by the rheometer. In this case, μ was calculated by applying the logarithmic fitting against the fluid temperature on the basis of the equation proposed by Kampmeyer and Girifalco. Curve fitting was also made against the shear rate based on the power law approximation. The properties were calculated in each experimental case applying the reference temperature and shear rate of the flow. The logarithm temperature of the channel was used as the reference temperature in the heat transfer measurement. $4U_m/D_h$ was applied as the reference shear rate. For reference, μ of the sucrose and PAAm solutions at the temperature of 20°C and shear rate of $10s^{-1}$ were μ=0.14 and 0.41 Pa·s, respectively. The relaxation time was measured by adjusting the general Maxwell model to the time history of the shear stress after a constant shear rate was suddenly applied to the fluid. In this case, the influence of the fluid temperature was taken into account. For reference, λ was in the range of 3.1~3.6s in the case of fluid temperature equal to 20°C.

The heat capacity C_p and thermal conductivity k used to obtain the heat transfer coefficient were derived from the empirical equation shown in the references of Gucker et al. (1937) and Werner et al. (2007) for the fluid temperature of 25°C.

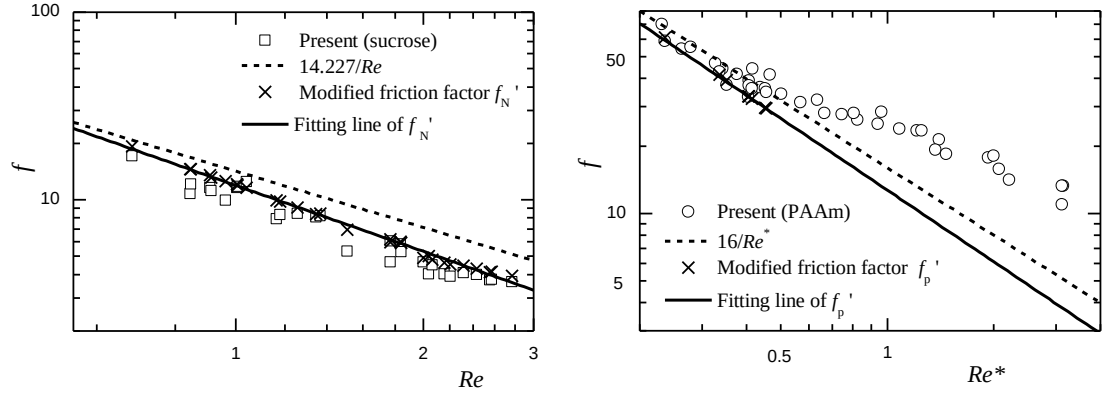

(a) Friction factor in sucrose case *(b) Friction factor in PAAm case*

Figure 3: Relationship between (a) friction factor and Reynolds number in the case of sucrose solution, (b) friction factor and modified Reynolds number in the case of PAAm solution.

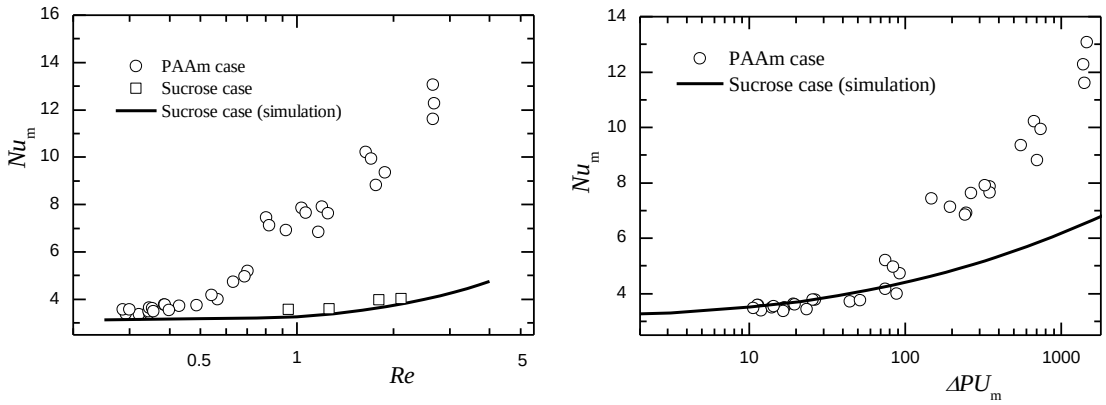

(a) Influence of Reynolds number *(b) Influence of pumping power*

Figure 4: Relationship between (a) average Nusselt number Nu_m and Reynolds number, (b) average Nusselt number Nu_m and the pumping power ΔPU_m.

2.6 Experimental conditions

The flow rate was changed in the experiments in order to examine the influence of the Reynolds number ($Re = \rho U_m D_h/\mu$) on the heat transfer coefficient, pressure loss and flow behavior in the channel. The conditions are summarized in Table 1. N_D shown in the table is the Dean number, which is defined as Eq. (5).

$$N_D = \mathrm{Re}\left(\frac{2D_h}{R}\right)^{0.5} \tag{5}$$

W is the channel width, and R_i and R_o are the inner and outer radii of the curved channel. Dean number can be used to assess the magnitude of the curvature effect on the flow structure, for example the generation of the Taylor-Dean vortices. Wi is the Weissenberg number and is defined as follows.

$$Wi = \lambda\left(\frac{4U_m}{D_h}\right) \tag{6}$$

3. Results and Discussion

3.1 Heat transfer and pressure loss characteristics

Figure 3 shows the friction factor distributions in relation to the Reynolds number *Re* and the modified value *Re** in the cases of sucrose and PAAm solutions. *Re** is a value defined as Eq. (7), which is used to rearrange the relationship with the friction factor in the case of power law fluids.

$$\mathrm{Re}^* = \frac{\rho U_m^{2-n} D_h^n}{8^{n-1} K\left(B + A/n\right)^n} \tag{7}$$

Constants *A* and *B* appearing in Eq. (7) are respectively 0.2121 and 0.6766 in the case of square duct [1].

The relationship between the friction factor and the Reynolds number can be described as follows. For the case of sucrose, which is Newtonian fluid, the correlation of f =14.2/*Re* is satisfied for the flow through a square duct. For the power law fluid flow, the relationship between f and *Re** can be shown as f =16/*Re** [1]. These correlations are shown by the dash lines in Figures 3 (a) and (b). Comparing these lines with the measurement results, one can see that the theoretical value over predicts the f distributions particularly in the case of sucrose solution. This is mainly attributed to the variation of the fluid property in the cross-sectional plane of the channel owing to the temperature distribution generated during the heat transfer measurement (the friction factor is measured simultaneously with the heat transfer measurement). This leads to the change of the velocity distribution in the cross-section. Although the temperature difference between the fluid and wall is not large, the high temperature dependency of the fluid mainly due to the sucrose produces such effect. In order to take this influence into account, f is modified using the following modification coefficient.

$$f_N' = \frac{14.2}{\mathrm{Re}}\left[\frac{\mu(T_w)}{\mu(T_m)}\right]^{\zeta}, \quad f_p' = \frac{16}{\mathrm{Re}^*}\left[\frac{\mu(\dot{\gamma}_m, T_w)}{\mu(\dot{\gamma}_m, T_m)}\right]^{\zeta} \tag{8}$$

The numerator and denominator are the fluid viscosities based on the wall and logarithm temperature of the fluid, respectively. ζ is constant and is 0.58 [12]. The results are shown in Figure 3 depicted by the solid line. In Fig. 3 (a), the measurement results and modified friction factor agree very well showing the validity of the present measurement. In Fig. 3 (b), the measurement results agree well with f_p' in the low *Re** area, the condition of which the flow is believed to be steady. As *Re** increases, the measurement result increases and deviates from f_p'. As will be discussed by the visualization results, the flow becomes unsteady as *Re* increases and large scale vortices are generated in the serpentine channel. The increase of f_p' is believed to be attributed to this change of the flow behavior.

The relationship between the average Nusselt number, Nu_m, and *Re* is shown in Fig. 4 (a). The solid line shown in the figure plots the numerical results of Chandrupatla et al. (1977), which presents the average Nusselt number of laminar flow in a square duct considering the entrance region effect. In this case also, we will modify the value by taking the temperature dependency of the fluid properties into account by applying the modification shown by Eq.(9).

$$Nu_N' = Nu_N\left[\frac{\mu(\dot{\gamma}_m, T_w)}{\mu(\dot{\gamma}_m, T_m)}\right]^{\xi} \tag{9}$$

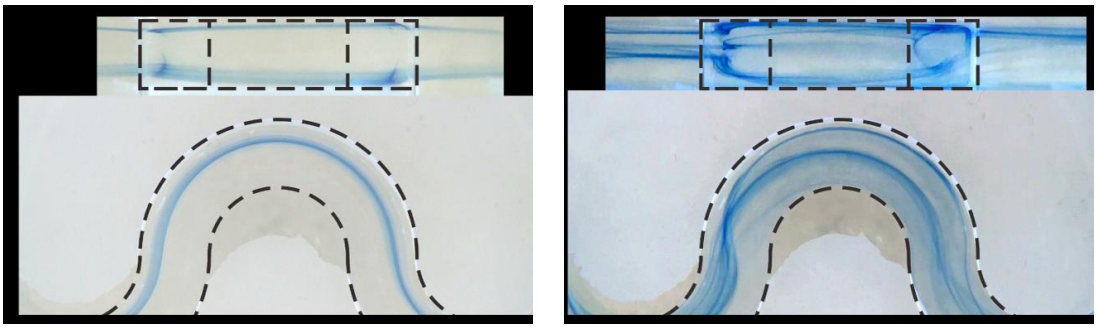

(a) Re=0.1, Wi=21.2, N_D=0.1 *(b) Re=1.3, Wi=184, N_D=1.1 (period 1)*

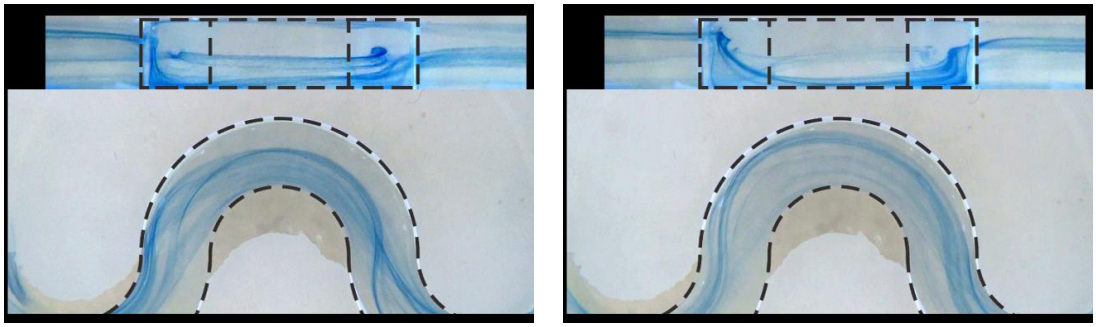

(c) Re=1.3, Wi=184, N_D=1.1 (period 2) *(d) Re=1.3, Wi=184, N_D=1.1 (period 3)*

Figure 5: Visualization of the streak lines at the 2nd curve of the serpentine channel in the PAAm solution case (measurement of the side and top views are synchronized).

ξ is constant and is -0.14 [12]. In Fig. 4 (a), the measurement results of the sucrose case agree well with the solid line confirming the validity of the measurement. On the other hand, Nu_m in the case of PAAm solution shows a similar value with the sucrose case in the region of Re <0.5. Then Nu_m increases as Re increases. The starting point of the increase of Nu_m matches with the one observed in the f distribution shown in Fig. 3 (b). Therefore, the increase of the heat transfer coefficient is believed to be attributed to the generation of the unsteady flow and vortices. At $Re \cong 2$, Nu_m in PAAm case takes 3 time greater value than the sucrose case showing an effective heat transfer enhancement.

As the f and Nu_m both increase, the relationship between Nu_m and the pumping power ΔPU_m is discussed in Fig. 4 (b). As shown in the figure, larger Nu_m is observed in the region where the flow becomes unsteady and vortices are generated. Therefore, when an equivalent pumping power is applied to the channel, larger heat transfer rate is obtained showing a high overall performance of the PAAm solution case.

3.2 Flow visualization

The streak lines visualized by the dye in the case of PAAm solution are shown in Fig. 5. Fig. 5 (a) shows the results of the flow under the lower Reynolds number condition (Re = 0.1), and (b) ~ (d) are the results of the same flow of Re = 1.3 each presenting the images at different time period. Visualized images taken from the side and top of the channel, which were recorded simultaneously, are both shown in each figure.

As shown in Fig. 5 (a), the streak lines flow along the channel and their relative positions to the channel cross-section are kept constant. Therefore, the flow is in steady state, and no noticeable secondary flows, such as Taylor-Dean vortices, are generated in the channel. As Re increases, the flow starts to fluctuate, and a strong secondary flow similar to a longitudinal vortex is observed in the channel particularly in the downstream area of the inflection point of

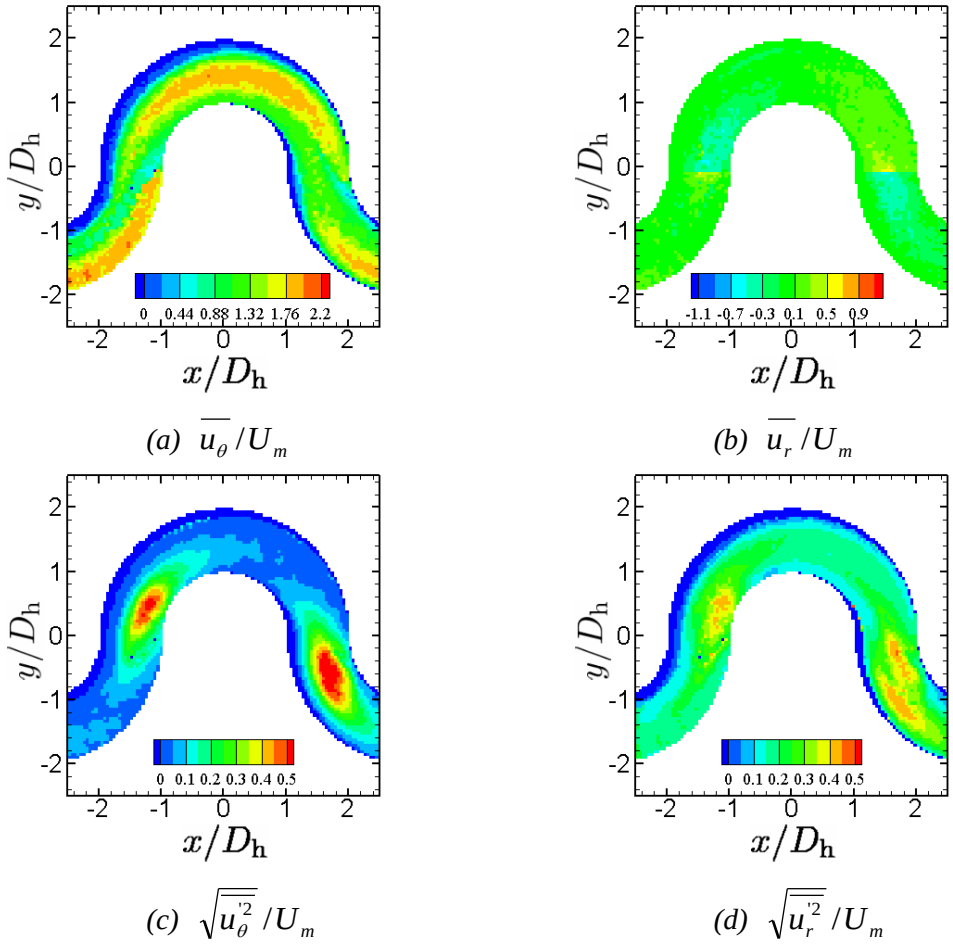

Figure 6: Mean velocity and fluctuation intensity distributions at the N = 2 curve in the case of PAAm solution (x-y plane at z = 0.5H, Re = 2.2, Wi = 120).

the serpentine channel. As Re increases Wi also increases. Since no such fluctuation or vortices were observed in the sucrose solution case even under high Re conditions, these phenomena are believed to be attributed to the increase of the normal stress owing to the viscoelasticity of the fluid as Wi increases. This will be discussed in the next section.

Comparing the patterns of the streak lines shown in Figures 5 (b) ~ (d), one can see that the vortices patterns differ with time. In Fig. 5 (b), downstream of the position $\theta = -90°$, two streak lines are observed. The one located at the upper side of the channel will move upwards and also inwards toward the inner side of the channel curve. The other one located at the lower side of the channel will move downwards and outwards as the dye flows downstream of the curved part. This streak pattern shows that a pair of longitudinal vortices is generated in the channel. In Figures 5 (c) and (d), all the streak lines located at the outside of the channel curve at $\theta = -90°$ moves downwards in the downstream area. The streak lines located at the upper half of the channel move outwards of the curve while the streak lines located at the lower half of the channel flow inwards. Therefore, the results show that a single anticlockwise vortex is generated in these cases. These pair and single vortices appear alternatively in the channel, which produces the fluctuation of the streak lines mentioned above.

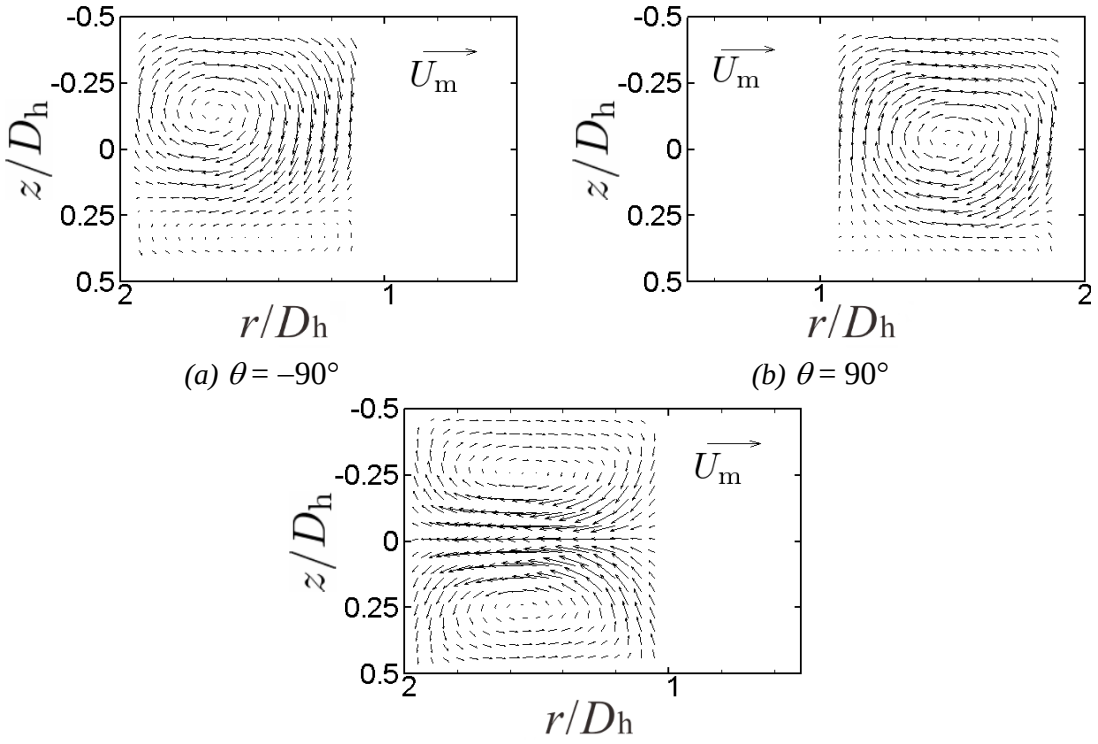

(a) $\theta = -90°$ *(b)* $\theta = 90°$

(c) $\theta = -78°$

Figure 7: Mean velocity distributions on the *x*–*z* plane measured at the *N* = 2 curve in the case of PAAm solution ((a) and (b): *Re* = 2.0, *Wi* = 333, (c): *Re* = 2.2, *Wi* = 319. Conditions are different due to the change in the fluid properties when the solution was prepared).

3.3 PIV measurement

Figures 6 (a) and (b) show the velocity distributions of the streamwise (circumferential) and spanwise (radial) components of the flow velocity measured on the *x*–*y* plane of the channel middle height at the 2nd curve of the serpentine channel. Figures 6 (c) and (d) show the fluctuation intensities.

Although not shown here, the spanwise velocities and the fluctuation intensities were nearly zero, and the streamwise velocity distributions showed a similar pattern with the sucrose solution case under the lower *Re* and *Wi* conditions. As shown in Figures 6 (c) and (d), as the flow rate increases the fluctuation intensities increase in the streamwise and spanwise directions. These values increase greatly particularly in the area downstream of the inflection point of the serpentine channel. This characteristic agrees well with the one observed in the flow visualization shown in Fig. 5.

Figures 6 (a) and (b) show that the main flow, the area of which the streamwise velocity takes its maximum value, flow along the outside of the curved channel and crosses the channel downstream of the infection point. The location of the area where the fluctuation intensities take their maximum peaks matches with this position. On the other hand, the spanwise velocity and the fluctuation intensities show considerably small value at the curved part ($\theta \cong 0°$). Larson et al. (1990) have reported that in the rotating co-axial cylinder case, Taylor vortices are generated in the curved channel due to the increase of the instability of the viscoelastic fluid flow. However, in the present case, the magnitude of the spanwise flow and intensities observed in the curve part was small indicating that no such vortex is generated. These might be attributed to twofold. The first one is the relatively small *Wi* number of the present study which is *Wi* ≅ 100. And the change of the curvature direction of the semi-circle

part can be another reason. Namely, the curvature direction could have changed before the vortex was able to develop due to the normal stress produced by the viscoelastic fluid.

Figure 7 show the mean velocity vectors on the $y - z$ plane (cross-section) measured at the streamwise positions of θ = –90°, –78° and 90°. In all figures, one can clearly find the generation of the longitudinal vortices. Comparing (a) and (b), the direction of the vortices are the same, and this trend was also observed in the instantaneous velocity distributions. This indicates that the vortex observed at θ =90° is not the one which was convected downstream from the location of θ =–90°. Further, the vortex generated at the infection point of the channel decays as it flows downstream in the curved area, and the generation of the next vortex starts when the flow reaches the next infection point.

Generation of a pair of vortices is observed in Fig. (c). As discussed in the previous sections, the Dean number N_D of the flow examined in this study is small, and indeed Dean flow was not observed in the sucrose solution case. Therefore, the pair of vortices observed in Fig. (c) can be attributed more to the normal stress difference of the viscoelastic fluid flow. As is well known, the curvature of the channel will produce a stress with a direction pointing toward the center of the curvature due to the normal stress difference, $(\tau_{11}-\tau_{22})/r$ [14]. As the fluid flows through the curve part, a force generating a flow flowing toward the inner side of the curve will work on the fluid in the area near the top and bottom walls due to the large shear stress. On the contrary, this force will be relatively small in the middle of the channel. Thus, the main flow located in the middle of the channel height will tend to flow through the outer sides of each curve as shown in Fig. 6 (a). This flow pattern will produce a flow crossing the channel in the area near the inflection point. This is believed to be one of the reasons for the generation of a pair of vortices observed in Fig. 7 (c). This flow and vortex structure change by time and leads to the fluctuation of the streak lines observed in Figures 5 (b)–(d). As described previously, the fluctuation of the spanwise component observed in Fig. 6 (d) is believed to be attributed mainly to this temporal behavior of the vortices.

From these measurements, the increase of the fluctuation intensities observed in Fig. 6 can be attributed to twofold. One is the fluctuation produced along the streamline as observed in the curved area shown in Fig. 6 (c). Since the flow crosses the channel near the inflection point, the fluctuation along the streamline will accompany an apparent spanwise fluctuation. The second one is the fluctuation due to the variation of the vortex pattern observed in Fig. 7. As mentioned in Section 3.2 and in above, the vortex changes its pattern from a single vortex to a pair of vortices with time. Even with the pair of vortices, the shape of the two vortices is not always symmetric. Further, the streamwise position and the direction of the vortices change. Such behavior of the vortices will consequently produce the flow fluctuation observed in Fig. 6. The heat transfer enhancement is, therefore, attributed not only to the unsteady flow, but also by the longitudinal vortex like secondary flow generated at the inflection point and the channel curve shown in Fig. 7.

4. Conclusions

Measurements of the heat transfer coefficient, flow visualization and flow velocity were carried out for the viscoelastic fluid flow in the serpentine channel with square cross-section. The conclusions obtained from the measurements are summarized as follows:

Enhancement of heat transfer performance was observed in the PAAm solution case compared with the sucrose solution case. The average Nusselt number Nu_m in the PAAm case increased markedly as the Reynolds number Re increased, and showed three times greater value at $Re \cong 3$. For the overall performance considering the pumping power, a larger Nu_m

was obtained with the same pumping power in the PAAm solution case compared with the sucrose solution case.

The streak lines visualized by the dye showed that steady flow was obtained when the *Re* (and *Wi*) was small in the PAAm solution case. As *Re* increases the flow starts to fluctuate and a generation of secondary flow was observed.

Streamwise fluctuation was observed along the serpentine channel in the PAAm solution case. Spanwise fluctuation, and also spanwise flows was, however, only observed in the area located downstream of the inflection point of the serpentine channel. In the same area, generation of longitudinal vortices was observed at the cross-sectional plane, which was believed to be attributed to the normal stress produced by the viscoelastic fluid. The variation of the vortex size and position was one of the reasons for the flow fluctuation.

5. Acknowledgements

This study was supported by the ministry of education, culture, sports, science and technology of Japan, and the authors acknowledge their financial support.

References

1. J. P. Hartnett and M. Kostic. Heat transfer to a viscoelastic fluid in laminar flow through a rectangular channel. *Int. J. Heat Mass Transfer*, 28: pp. 1147-1155, 1985.
2. X. Chunbo and J.P. Hartnett. Influence of rheology on laminar heat transfer to viscoelastic fluids in a rectangular channel. *Ind. Eng. Chem. Res.*, 31: pp.727-732, 1992.
3. Y. L. Joo and E. S. G. Shaqfeh. Observation of purely elastic instabilities in the Taylor-Dean flow of a Boger fluid. *J. Fluid Mech*., 262: pp. 27-73, 1994.
4. R. G. Larson, E. S. G. Shaqfeh and S. J. Muller. A Purely Elastic Instability in Taylor-Couette flow, J. Fluid Mech., Vol. 218, pp. 573-800, 1990.
5. A. Groisman and V. Steinberg. Efficient mixing at low Reynolds numbers using polymer additives. *Nature*, 410: pp. 905-908, 2001.
6. B. Teodor, S. Enrico, A. Groisman and V. Steinberg. Chaotic flow and efficient mixing in a microchannel with a polymer solution. *Physical Review E*, 69: p. 066305, 2004.
7. S. Tamano, M. Itoh, A. Sasakawa and K. Yokota. PIV Measurement of secondary flow in curvilinear pipe flow of polymer solution, *Trans. of JSME part B*, 75: pp. 2115-2121, 2009.
8. R. K. Shah and A. L. London. *Laminar flow forced convection in ducts, advances in heat transfer*, Supplement, Academic Press, 1978.
9. C. L. Wiginton and C. Dalton. Incompressible laminar entrance flow in a circular sector duct. *J. Appl. Mech*, 37: pp. 854-856, 1970.
10. F. T. Gucker and F. D. Ayers. The Specific heat of aqueous sucrose solutions at 20ºC and 25ºC and the apparent molar heat capacity of non-electrolytes. *J. American Chem. Society*, 59: pp. 447-452, 1937.
11. M. Werner, A. Baars, F. Werner, C. Eder and A. Delgado. Thermal conductivity of aqueous sugar solutions under high pressure. *Int. J. Thermophys.*, 28: pp. 1161-1180, 2007.
12. W. N. Kays and M. E. Crawford. *Convective heat and mass transfer, second edition*, pp. 275-287, McGraw-Hill, 1980.
13. A.R. Chandrupatla and V. M. K. Sastri. Laminar Forced Convection Heat transfer of a non-Newtonian fluid in a square duct. *Int. J. Heat Mass Transfer*, 20: pp. 1315-1324, 1977.
14. R. B. Bird, R. C. Armstrong, and O. Hassager. *Dynamics of polymer liquids: volume 1 fluid mechanics (2nd ed.)*. Wiley-interscience, 1987.